Fusion and transfer reactions in the $^{19}F + ^{165}Ho$ system at energies near the Coulomb barrier

A. Navin, A. Chatterjee, S. Kailas, A. Shrivastava, P. Singh, and S. S. Kapoor
Nuclear Physics Division, Bhabha Atomic Research Centre, Bombay 400 085, India
(Received 30 November 1995)

Results of the measurements of fusion cross sections and average angular momenta in the $^{19}F + ^{165}Ho$ system, for center-of-mass energies ranging from 7 MeV below to 13 MeV above the Coulomb barrier are presented. The average angular momenta of the compound system were obtained using three independent methods, namely, the γ-ray multiplicity, the ratios of the evaporation residues, and the fusion excitation function. The transfer probabilities for various one- and two-particle channels have also been measured at a beam energy of 110 MeV, an energy much higher than the Coulomb barrier. The measured Q-integrated one- and two-proton transfer probabilities have been analyzed in terms of an earlier suggested semiclassical calculation taking into account the nuclear branch in addition to the usual Coulomb branch of the classical deflection function. It is seen that the ''slope anomaly'' in the measured one- and two-proton transfer probabilities as a function of the distance of closest approach can be explained within this framework. The strengths of the form factors, required in a coupled channel calculation of fusion, for the important transfer channels were obtained from the data within such a semiclassical analysis. The observed enhancement of the fusion cross sections and average angular momenta is discussed in terms of the coupled channel model using static deformation for the target, inelastic excitations in the projectile, and couplings to the transfer channels. The data are also compared with the neutron flow model suggested by Stelson. [S0556-2813(96)00607-3]

PACS number(s): 25.70.Jj, 25.70.Hi

I. INTRODUCTION

While heavy-ion fusion is reasonably well understood for energies above the Coulomb barrier, the measured fusion cross sections at below-barrier energies are much larger than those expected on the basis of a one-dimensional barrier penetration model (1D-BPM) [1,2]. The corresponding angular momentum distributions are also found to be broader than those expected from these models. The angular momentum distributions of the compound system (or its moments) have been derived from various methods like γ-ray multiplicities, the relative yields of the evaporation residues formed in the decay of the compound nucleus, fission fragment angular distributions, isomer ratios, etc. [3]. It is generally believed that the angular momentum distributions and the fusion cross sections act as independent constraints for fusion models. A model-independent relationship suggested [4,5] between the fusion excitation function and the angular momentum distribution is of great importance as the validity of this relationship leads to constraints on fusion models. A comparative study of the average angular momentum extracted by various methods in the same system would be interesting as consistency among them indicates validity of the assumptions involved.

Heavy-ion transfer reactions around the barrier are of interest both for understanding the transfer process [6,7] as well as for its connection with subbarrier fusion enhancement [8]. Semiclassical concepts have been extensively used in the study of heavy-ion reactions [9]. The WKB [10] approximation provides a way to relate particle properties (classical trajectories) to wave properties (semiclassical wave functions). Apart from leading to greater physical insight and localizations of the contributions, calculations are simpler in a semiclassical approach. The study of the various channels like elastic, inelastic, few-nucleon transfer, and fusion shows that a particular process should not be treated in isolation; for example, the threshold anomaly in elastic scattering was shown to be connected to near-barrier fusion enhancement [11]. The interconnectivity of various channels is a compelling reason for the use of a coupled channel approach. As the number of channels to be coupled to the elastic channel is increased, calculations tend to become intractable in a quantum mechanical approach. A semiclassical approach by the virtue of the equations being first order would be better suited for coupled channel computations.

For understanding the fusion phenomenon, the coupled channel formalism with simplifying approximations has been widely used [12]. The WKB approximation is employed in most fusion calculations for obtaining the transmission coefficients. Usually an ''experimental'' approach is adopted in determining the types and number of channels to be coupled. The measurement of the transfer channels is necessary to obtain the coupling strengths, which in turn require a measurement of quasielastic scattering. One should try to understand these processes consistently. The couplings to the inelastic channels are well understood but the strengths of the couplings to the transfer channels are obtained empirically. Microscopic calculations for the single-particle form factors have been made for some cases [13] and macroscopic form factors for pair transfers have also been suggested [14]. In the present work we have obtained the strengths from the measured transfer angular distributions from above-barrier data. The extraction of the strengths is easier from subbarrier data, although measurements of these low cross sections are more difficult. The strengths are obtained after explaining the slope anomaly as shown in a recent work [15] and hence can be considered to be an improved estimate.

The system $^{19}F + ^{165}Ho$ was chosen for the present investigation as it offers several advantages. Among others the role of static deformation in the fusion mechanism is an im-

portant one and ^{165}Ho has a very large deformation. The γ-ray decay schemes of the evaporation residues from the compound system are well studied, the evaporation residues from the compound system ^{184}Os are good rotors and do not have any high-spin isomers, making the conversion from multiplicity to angular momentum relatively simple. In the energy range of interest the evaporation residues exhaust almost all the fusion cross section because of a large fission barrier and the monoisotopic nature of Ho makes the measurements cleaner. Recently Christely *et al.* [16] made a coupled channel calculation for fusion of ^{16}O on aligned Ho where they showed that the effect of alignment on the fusion cross section is considerable.

We report here measurements at energies around the Coulomb barrier of the fusion cross sections and the average angular momenta which were obtained from the γ-ray multiplicity, evaporation residue ratios, and the fusion excitation function under some simple assumptions. Angular distributions for various transfer channels were made in an angular range corresponding to large distances of closest approach for Coulomb trajectories at energies of 110 and 70 MeV. The transfer data have been analyzed within a semiclassical framework incorporating the nuclear branch in addition to the Coulomb branch of the classical deflection function. The results of the fusion measurements have been compared with the coupled channel model incorporating static deformation, transfer and inelastic channels, and also the Stelson model [17].

II. EXPERIMENTAL DETAILS AND RESULTS

A. Transfer measurements

The experiments were performed using ^{19}F beams from the BARC-TIFR Pelletron accelerator facility at Bombay. The ^{165}Ho target ($\simeq$250 μg/cm^2) was made by vacuum evaporation on a carbon backing ($\simeq$40 μg/cm^2). Measurements were made at laboratory energies of 110 MeV and 70 MeV corresponding to energies $1.38V_b$ and $0.88V_b$, where V_b is the Coulomb barrier. Three Si surface barrier telescopes (17 μm and 2 mm, 11 μm and 2 mm, 12 μm and 2 mm) were used in a 1 m diameter stainless steel scattering chamber [18] to measure the angular distributions of the beamlike transfer products. For the 110 MeV data $\Delta\theta$ was reduced to 0.6° from 1.4° used for the 70 MeV data. A 300 μm Si surface barrier detector placed at 25° with respect to the beam direction was used for normalization purposes. The angular range covered mainly corresponded to large distances of closest approach for Coulomb trajectories. At 110 MeV the angular range was 32.5°–54.5° and at 70 MeV was 125.5°–165.5°. The data were collected in two-dimensional (2D) ΔE vs E arrays of size 512×512 using a transputer-based multiparameter data acquisition system [19]. After off-line gain matching of the ΔE and E data, 2D plots of ΔE vs E_{total} and particle identifier (PI) vs E_{total} were generated. The algorithm for particle identification had the form $M^{a-1}z^2 \propto(\Delta E+E)^a-E^a$, where a value of $a = 1.65$ was used to linearize the plots in the energy range of interest. The numerical value of a was obtained using the range-energy tables of Northcliff and Schilling [20]. The PI calibration was additionally verified using an elastically scattered 70 MeV ^{12}C beam. A typical ΔE-E_{total} plot at a bombarding energy of 110 MeV is shown in Fig. 1. The energy resolution for the elastic peak was $\simeq$ 800 keV. The various z and mass groups can be identified in the figure. The vertical band seen near the elastic energy is due to the nonuniformity of the ΔE detector and represents less than 0.5% of the total counts. Shown in Fig. 2 is the PI spectrum for the data in Fig. 1. The various channels can be clearly identified. For the data taken at much lower energies, mass separation was not possible. We have earlier reported the transfer probabilities at energies of 75, 80, 85, and 90 MeV where only charge separation was possible [21]. A typical Q-value spectrum for the $1p$ channel is shown in Fig. 3. The optimum (Q_{opt}) and

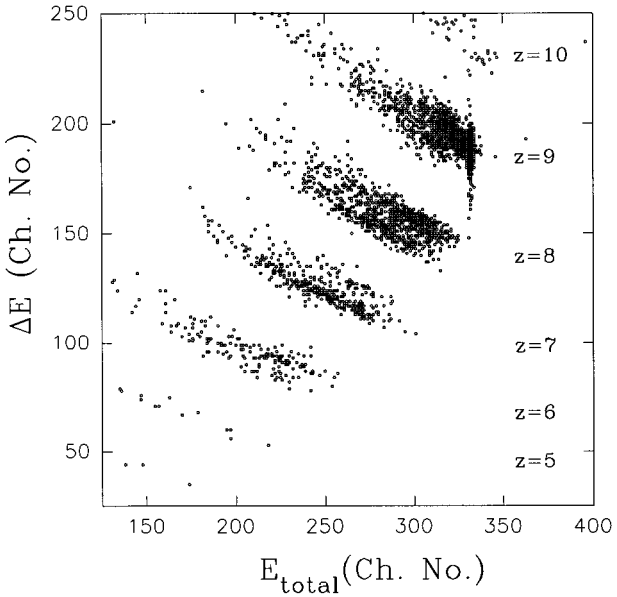

FIG. 1. A typical two-dimensional spectrum of ΔE vs E_{total} at a bombarding energy of 110 MeV. The various z groups are indicated.

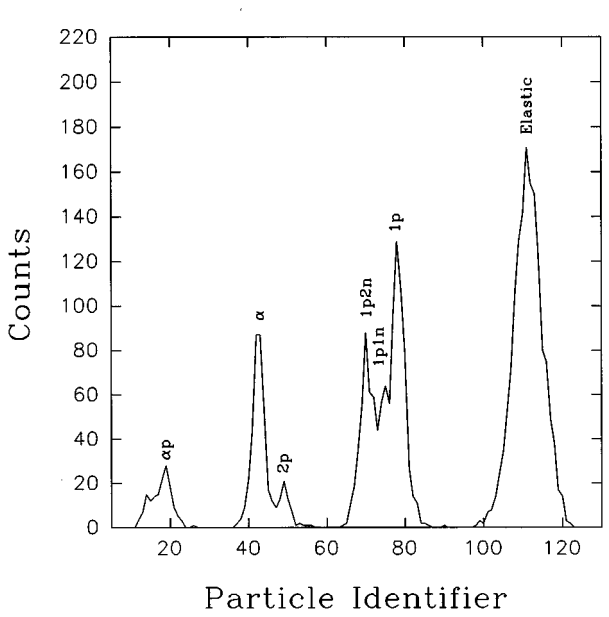

FIG. 2. A particle identifier spectrum of the data shown in Fig. 1. The peaks are labeled by the transfer channels they arise from.

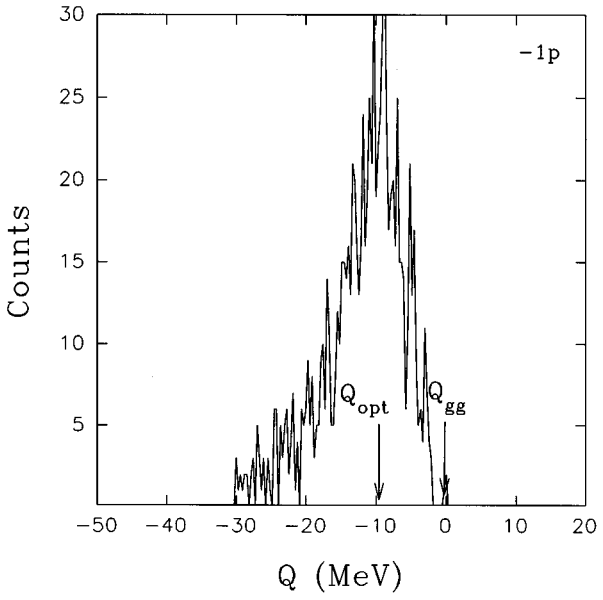

FIG. 3. A typical Q-value spectrum for the one-proton stripping channel. The ground state Q value (Q_{gg}) and Q_{opt} (see text) are shown.

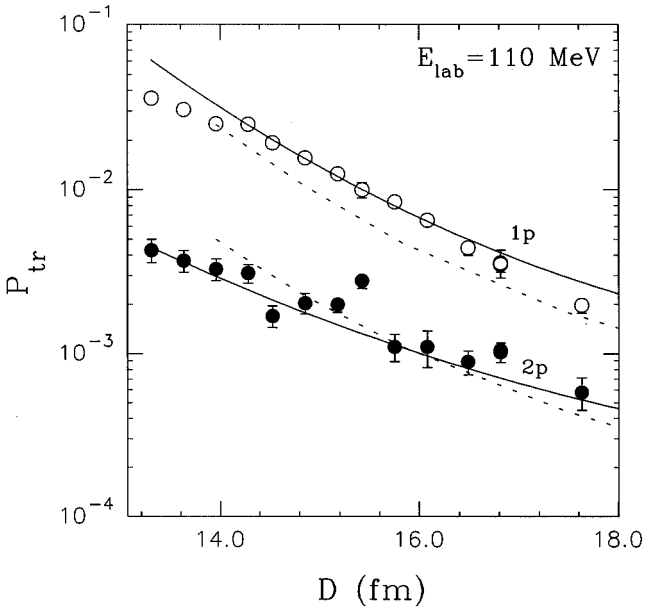

FIG. 4. Transfer probabilities (defined in text) for one- and two-proton transfer at 110 MeV, as a function of the distance of closest approach, D, for a Coulomb trajectory. The solid lines are the results of semiclassical calculations using (13) for one-proton and two-proton transfer. The dashed lines are calculated from (14).

ground state (Q_{gg}) Q values are indicated. The shape of the Q-value spectrum is seen to be Gaussian. The peaking at $Q_{\rm opt} = E_{\rm c.m.}[(z^f Z^f/z^i Z^i)-1]$ arises in semiclassical models from trajectory matching conditions (i and f refer to the incoming and outgoing channels, respectively). The transfer probability $P_{\rm tr}$ is defined as the ratio of the Q-integrated transfer cross sections $\sigma_{\rm tr}$ to the quasielastic (sum of elastic, inelastic, and transfer) cross sections $\sigma_{\rm qe}$. (This usage of the term ''quasielastic'' differs from that in [6] where quasielastic reactions include only inelastic and few-nucleon transfer and not elastic scattering.) Shown in Fig. 4 are the transfer probabilities for one- and two-proton stripping channels at 110 MeV as a function of the distance of closest approach, D, for a Coulomb trajectory,

$$D=\frac{z_p Z_t e^2}{2E_{\rm c.m.}}\left(1+\csc\frac{\theta_{\rm c.m.}}{2}\right). \tag{1}$$

This is done so as to be consistent with the usual convention, although we show later that there are at least two branches (distances) contributing to a given scattering angle for energies much above the Coulomb barrier. The transfer probabilities for the z_p-1 and z_p-2 transfer channels at 70 MeV are shown in Fig. 5. The error bars shown correspond only to statistical errors. As can be seen from Fig. 4 for the above barrier data at 110 MeV the one- and two-proton transfer probabilities have nearly the same slope contrary to simple expectations based on binding energy considerations. This is the ''slope anomaly.'' We shall show in Sec. III how this can be understood by taking into account the various branches of the classical deflection function as shown in a recent work [15]. As the data at 70 MeV are not mass separated it would be difficult to comment on the differences in the slopes of Fig. 5. The slopes for the one- and two-particle transfer channels are expected to be different in the 70 MeV case, as below the Coulomb barrier [22] only the Coulomb branch is expected to contribute.

B. Fusion measurements

1. Cross section

The measurements were made in the energy range 72–95 MeV. Targets ($\simeq$250 μg/cm^2) were made by vacuum

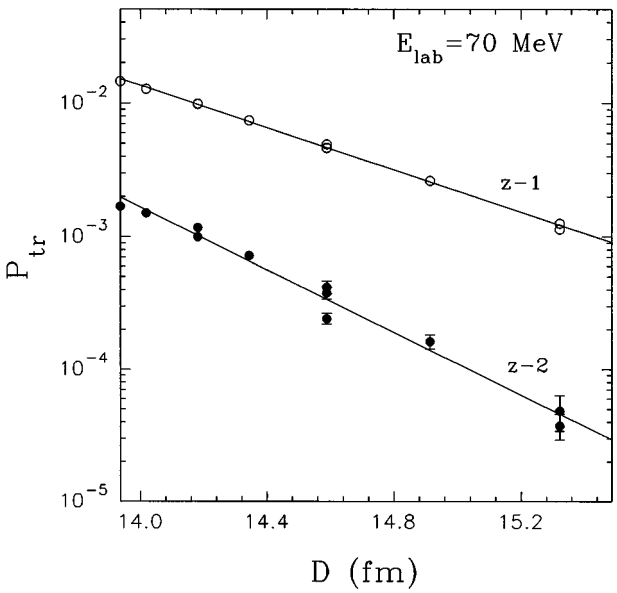

FIG. 5. Transfer probabilities for $z-1$ and $z-2$ transfer channels at 70 MeV, as a function of the distance of closest approach, D, for a Coulomb trajectory. The lines are to guide the eye.

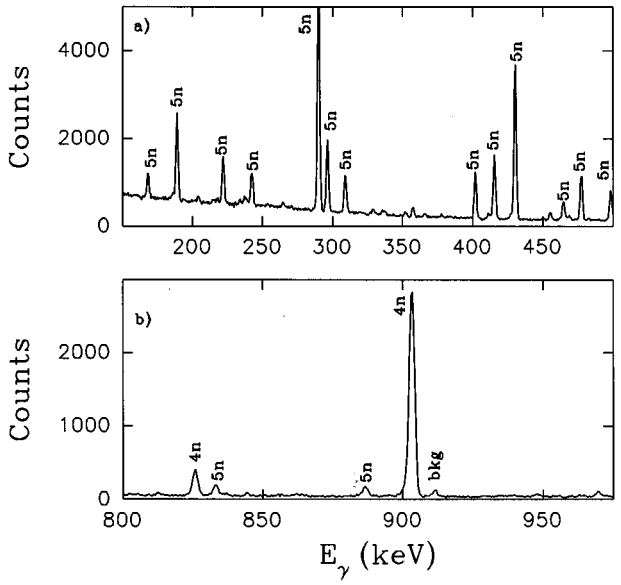

FIG. 6. An off-beam γ-ray spectrum following irradiation at 90 MeV. Shown in (a) and (b) are two different regions of the spectrum. The labels on the γ peaks indicate the evaporation residue channels they arise from.

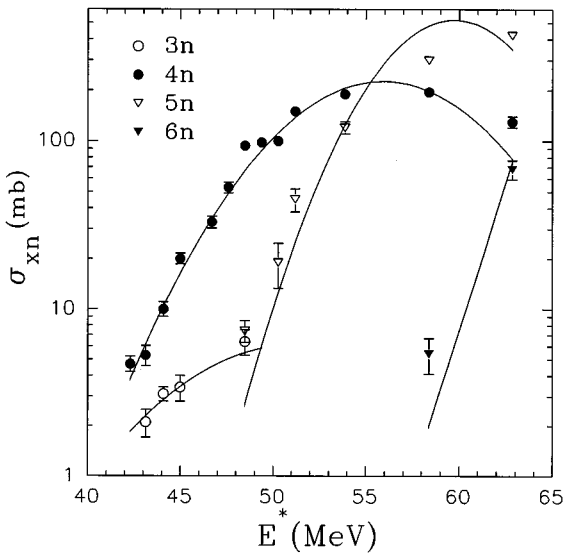

FIG. 7. The partial evaporation residue cross section as a function of the excitation energy. The open circles, solid circles, open triangles, and solid triangles represent the $3n$, $4n$, $5n$, and $6n$ cross sections, respectively. The lines are results of CASCADE calculations for the various channels.

evaporation of Ho on rolled Al (1 mg/cm^2), natural Pb (4 mg/cm^2), and C ($\simeq$40 μg/cm^2) backings for the cross section, γ-ray multiplicity, and fission measurements, respectively. The total fusion cross sections at various energies (fusion excitation function) were determined from the sum of the cross sections of the various evaporation residues. The fission fragment angular distribution was measured at $E_{\rm lab}$ of 95 MeV. The fission cross section was determined to be about 3 mb, confirming that it is indeed small. The measurements were made in an angular range 80°–170° in the laboratory. The fission fragments were measured in a gridded gas ionization detector (ΔE) followed by three surface barrier (E) detectors and three independent surface barrier telescopes. The evaporation residue cross sections were obtained from the off-line measurement of their γ decay with an efficiency calibrated 125 cm^3 HpGe detector. The HpGe detector was placed in a stainless steel insert with a thin window at a distance of 13 cm from the target in the scattering chamber. Two particle detectors placed symmetrically on either side of a well-collimated beam were used for absolute normalization. The lowest-energy points were measured in another setup with a small chamber where the target was removed for off-line counting. Target thickness was estimated by x-ray fluorescence in comparison with a standard sample and also by measuring the elastic scattering cross sections at forward angles. The beam current was measured in a multiscaling mode at 30 s intervals to monitor the variation of beam intensity. The evaporation residue cross sections for the $3n$-$6n$ channels were obtained from their radioactive decay [23]. The charged particle channels are predicted to be a small fraction of the total and have not been considered. In the low-energy measurements the counting was done at several intervals to follow the half-lives of the evaporation residues to ensure against any contamination of the γ-ray peaks of interest arising from other sources. A typical γ-ray spectrum is shown in Fig. 6. Shown in Fig. 7 are the individual *xn* channels as function of the excitation energy. The solid lines are calculations made with the statistical model code CASCADE [24] for the various evaporation residues, using the parameter set described below. The fusion cross sections plotted as a function of the center-of-mass energy are shown in Fig. 8.

2. Average angular momentum

The average angular momenta have been obtained by three different methods.

a. From γ-ray multiplicity measurements. The γ-ray fold distributions (the number of detectors firing in coincidence with an identified fusion product) were measured at laboratory energies of 75 MeV and 90 MeV, using an array of 14 hexagonal BGO detectors [25] (each 63 mm by 57 mm) in coincidence with a HpGe detector. Two sets of seven BGO's in a close-packed geometry were placed symmetrically above and below a thin target chamber, followed by a beam dump 2 m away. The total efficiency was measured to be 0.65 $\pm$ 0.02 using calibrated sources. The threshold of each detector was set to be $\simeq$100 keV. The individual efficiencies of all the detectors were made equal by configuring them suitably. The data were collected in an E_γ-fold matrix of size $4k\times128$. The data were hardware gated by the prompt of the TAC between the HpGe and the OR's of the BGO's. The random coincidences were found to be a negligible fraction of the true events. The multiplicity was obtained from the fold distribution for each channel by convoluting in the detector response following the formalism discussed in the literature [26]. The average multiplicity for each channel was converted to angular momentum by using a general expression as given in [27],

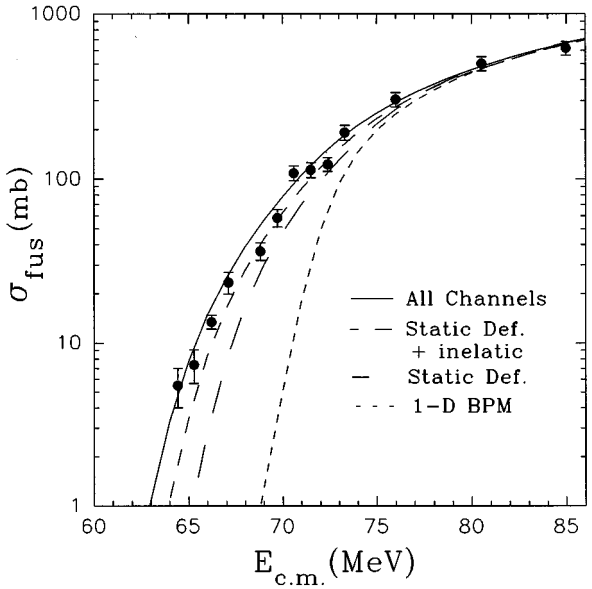

FIG. 8. The experimental fusion cross section as function of the center-of-mass energy in the $^{19}F + {}^{165}Ho$ system. The short dashed line shows the prediction of a 1D BPM calculation using the parameters given in the text. The long dashed line is a coupled channel calculation taking into account only the static deformation of the target. The medium dashed line is a coupled channel calculation including the coupling to the projectile inelastic excitations in addition to the static deformation of the target. The solid line shows the results of the complete coupled channel calculations described in Sec. III.

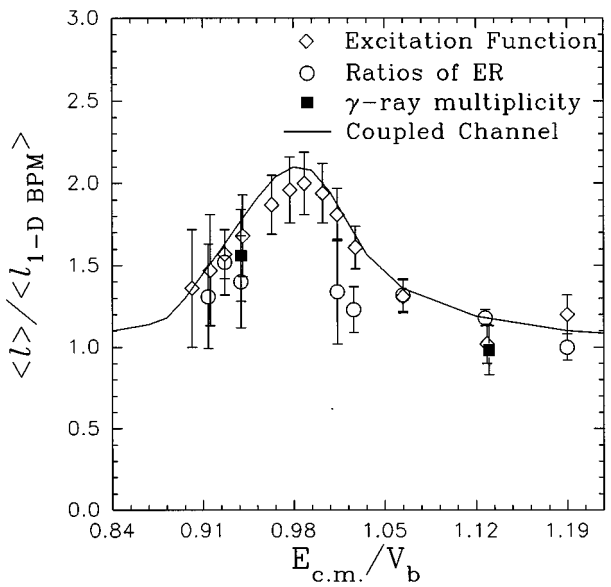

FIG. 9. The ratio of the average angular momentum to the 1D BPM prediction, obtained from the different methods as a function of $E_{\text{c.m.}}/V_b$. The solid squares are from γ-ray multiplicity measurements, the open circles are derived from the ratios of the evaporation residue yields, and the open diamonds are obtained from the fusion excitation function. Also shown are the coupled channel calculations corresponding to the solid line in Fig. 8.

$$\langle l\rangle = \Delta I_{\text{ns}}(\langle M_\gamma\rangle + 1 + BB - \langle M_{\text{stat}}\rangle) + \Delta I_s\langle M_{\text{stat}}\rangle + \Delta J_n\langle M_n\rangle + J_h, \tag{2}$$

where ΔI_{ns} and ΔI_s are the average angular momenta of nonstatistical and statistical γ rays, $\langle M_\gamma\rangle$ and $\langle M_{\text{stat}}\rangle$ are the measured and statistical γ-ray multiplicities, BB is a correction for unobserved γ rays, and J_h is the bandhead spin. BB and J_h are obtained from knowledge of the level schemes.

The average angular momentum for each channel was obtained using (2). The residual Os nuclei are good rotors and the γ-ray transitions are assumed to be of the stretched type. Values for ΔI_{ns} of $2\hbar$ and $1.5\hbar$ were used for the even and odd evaporation residues, respectively. The angular momentum of the compound nucleus was obtained by weighing the average angular momentum of each channel l_{xn} by its partial cross section σ_{xn},

$$\overline{l} = \frac{\Sigma\sigma_{xn}\overline{l_{xn}}}{\Sigma\sigma_{xn}}. \tag{3}$$

The results of these measurements are represented by the solid squares in Fig. 9 where the ratio of the measured l to that obtained from a 1D BPM is plotted as a function of $E_{\text{c.m.}}/V_b$. Since there are large number of detectors, the experimental error in the derived M_γ is small. The errors arise mainly due to uncertainty in the conversion from M to l.

b. From the ratios of the measured evaporation residues using a statistical model. At a given excitation energy of the compound nucleus, the relative fractionation into different evaporation residues depends on the angular momentum distribution with which it is formed apart from factors such as density of the final state and barrier penetration [28]. The effect of the shape of the distribution was also studied and as shown earlier the results are not very sensitive to it. Analysis of several systems using this method has been made [29]. In the present work the average angular momenta were derived from the measured $4n/5n$ and $3n/4n$ evaporation residue ratios using the statistical model code CASCADE. A Gaussian distribution for σ_l of the form $e^{-(l-l_0)^2/2\sigma^2}$ with $\sigma = 0.5l_0$ was taken. This was done for ease of calculation; in principle, one can obtain the ratios for each l weighted by a distribution. The distribution was obtained from an analysis of nearby systems where the angular momentum distribution has been measured. Simultaneous explanation of more than one evaporation ratio at a given excitation energy serves as a check on the assumed l distribution. The l was obtained by matching the calculated ratios with the experimental ones. The optical potentials for obtaining the transmission coefficients have been taken from Perey [30] for protons, Wilmore and Hodgson [31] for neutrons, and Huizenga and Igo [32] for alpha particles. The back-shifted Fermi gas model of Dilg *et al.* [33] was used for the level densities with $a=A/8.5$ MeV^{-1}. As a test of the above parameter set it was confirmed that the l obtained from the ratios of evaporation residue yields [34] in three systems leading to the compound nucleus ^{182}Os were in agreement with those obtained from γ-ray multiplicity measurements [27]. The open circles in Fig. 9 represent the l obtained from the evaporation residues. The errors in the derived average angular momentum reflect the errors in the measured ratios only. At the lower energies

the sensitivity of the ratios to $\overline{l}$ is smaller. The extracted $\overline{l}$ depends upon the statistical model parameters like the level density parameter a used in the analysis. However, the sensitivity to a is reduced at higher excitation energies and angular momenta.

c. From the fusion excitation function. It was pointed [4,5] out that under some simple conditions (4)–(7), the two observables, angular momentum and fusion cross sections, are not independent and one can derive a relationship between $\overline{l}$ or $\overline{l^2}$ and the fusion excitation function which is model independent. The fusion cross section is given by the sum of the partial wave cross sections σ_l given by

$$\sigma_l(E)=\frac{\pi\hbar^2}{2\mu E}(2l+1)T_l(E), \tag{4}$$

$$\sigma(E)=\sum \sigma_l(E), \tag{5}$$

where μ is the reduced mass, E the center-of-mass energy, and $T_l(E)$ are the transmission coefficients for fusion, for the lth partial wave. Dasso *et al.* [4] and Balantekin and Reimer [5] pointed out that if these transmission coefficients follow the relationship

$$T_{\ell}(E)=T_0(E'), \tag{6}$$

with

$$E'=E-\frac{\ell(\ell+1)\hbar^2}{2\mu R_b^2}=E-\beta(E)\ell(\ell+1), \tag{7}$$

where R_b is the barrier radius, $\overline{l}$ can then be expressed as

$$\overline{\ell}=\frac{1}{2E\sigma(E)\beta^2(E)}\int_{-\infty}^{E}\frac{\sigma(E')E'\beta(E')}{((E-E')/\beta(E)+1/4)^{1/2}}dE'. \tag{8}$$

Using the above relation involving an integral of $\sigma(E)$ the $\overline{l}$ and/or $\overline{l^2}$ can be derived. Equations (6) and (7) have been separately tested earlier [29]. The conclusion that was drawn from these analyses is that the agreement between the $\overline{l}$ values obtained from the direct measurements and those derived from the fusion excitation function is quite good. The major discrepancies occur for the cases where $\overline{l^2}$ values were obtained from fission fragment angular distributions. In a recent work it was shown that the $\overline{l^2}$ for the $^{16}O+^{208}Pb$ system are indeed consistent with those obtained from the fusion cross sections [35]. The average angular momenta $\overline{l}$ were calculated from (8) by numerical integration using interpolated and extrapolated values of the fusion cross sections. For this purpose the cross sections at the required energies were obtained by logarithmic interpolation of the measured values. For simplicity, no energy dependence of $\beta(E)$ was used. Since in the case of a deformed target there is an R_b associated with each orientation, a weighed average of R_b has been taken. The results obtained are shown in Fig. 9 by open diamonds. We have indicated representative error bars in Fig. 9, based only on the errors in the cross sections. Consideration of correlation of the errors among the various terms in the numerical integration would result in smaller error assignments.

III. COMPARISON WITH THEORETICAL MODELS AND DISCUSSION

A. Transfer

1. Semiclassical formalism and analysis

The transfer probability is defined as the ratio of differential cross sections for transfer and quasielastic scattering. For large distances of closest approach, in a semiclassical model, the transfer probability is expected to depend only on the tails of the wave functions of the transferred particle and the other nucleus, and have a near exponential falloff with the angle-dependent distance D of closest approach. It can be expressed as

$$P_{\rm tr}(D)=P_{\rm tr}(D_0)e^{-2\alpha(D-D_0)}, \tag{9}$$

where D_0 is a scale parameter, taken as $D_0=1.4(A_P^{1/3}+A_T^{1/3})$ fm, $\alpha=(1/\hbar)\ (2\mu B)^{1/2}$ where μ and B are the reduced mass and the binding energy, corrected for Coulomb effects, of the transferred particle(s) in the target and projectile. Based on the above arguments the two-nucleon transfer probability is expected to fall twice as fast as the one-nucleon probability as a function of the distance of closest approach (D). Experiments [36] show for energies above the Coulomb barrier that the two slopes are nearly similar. The observed deviation from the expected behavior is referred to as the slope anomaly. This has been interpreted as the failure of the applicability of a semiclassical treatment for energies above the Coulomb barrier and has been attributed to the importance of diffractive effects at these energies [36,37]. Semiclassical methods have been used to explain diffractive effects quite successfully [38,39]. The real trajectories provide a good approximation to the quantal wave when the potential has no sizable variation within the wavelength λ. If diffractive effects and complex potentials irrespective of their strength are to be treated, then inclusion of the complex solutions of the Hamilton-Jacobi equations is necessary [38]. An approximate method to treat a complex potential is to use the trajectory defined by the real part of the potential and treat the effect of the imaginary part as an attenuation factor along the trajectory [40]. This holds if the imaginary part of $(V(r)/[E-V(r)])$ is small along the trajectory. Recently [15] we have shown that the slope anomaly can be understood within the semiclassical framework by taking into account the nuclear branch of the classical deflection function in addition to the usual Coulomb branch. In the present work we have followed this perturbative approach.

The classical deflection function (relation between the impact parameter b or orbital angular momentum l and the scattering angle θ) is required for the analysis of the (quasi)-elastic scattering. The deflection function, obtained from a solution of classical equations of motion, is calculated from

$$\theta(L,E)=\pi-2L\int_{r_0(E)}^{\infty}\frac{dr}{r^2p(r)}, \tag{10}$$

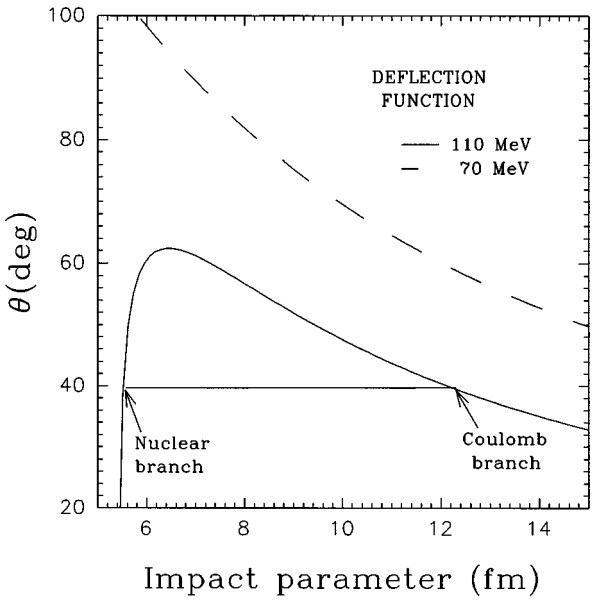

FIG. 10. The classical deflection function obtained from (10) calculated with a real optical potential at 70 MeV (dashed line) and 110 MeV (solid line). The Coulomb and nuclear branches are indicated for a typical angle.

where $p(r)$ is the radial momentum, L is $(l+1/2)\hbar$, and $r_0(E)$ is the outermost turning point which is a solution of the equation $E-V(r,L)=0$ for a given energy E and angular momentum L. Deflection functions obtained using (10) are shown at 70 and 110 MeV in Fig. 10. Denoted in the figure for a typical angle are the two contributions arising from two different impact parameters labeled as Coulomb and nuclear branches. The real part of the optical potential for the calculation was $V_0=45$ MeV, $R_0=9.6$ fm, and $a_0=0.8$ fm. This potential is shallower and more diffuse than the one used in the fusion calculations (Sec. III B) but has nearly the same value near the strong absorption radius. The justification for a larger value of diffuseness has been discussed earlier [15]. The (quasi)elastic scattering cross sections are obtained from

$$\frac{d\sigma}{d\Omega}=\frac{b}{\sin\theta}\frac{db}{d\theta}. \tag{11}$$

The transfer process is treated as a perturbation to (quasi)-elastic scattering and the transfer cross section can be written as

$$\left(\frac{d\sigma_{\rm tr}}{d\Omega}\right)=\sigma_{\rm el}P_{\rm tr}, \tag{12}$$

where $\sigma_{\rm el}$ is the (quasi)elastic cross section and $P_{\rm tr}$ is the transfer probability.

The classical deflection function for energies much above the barrier (110 MeV), such as the one shown in Fig. 10, shows that the contributions to a given deflection angle arise from more than one impact parameter or distance of closest approach. While computing the cross section for a given scattering angle, contributions arising from the various different impact parameters should be taken into account. Correspondingly for energies much lower than the barrier (70 MeV) the deflection function is a monotonically increasing function for decreasing values of the impact parameter (b) as shown in Fig. 10. The transfer probability can be expressed as [15] an incoherent sum of the contributions arising from the Coulomb and nuclear branches, ignoring the negative angle contributions which are strongly absorbed:

$$P_{\rm tr}(D)=P_{\rm tr}(D_{\rm nucl})\frac{\sigma_{QE(\rm nuc)}}{\sigma_{\rm QE}}+P_{\rm tr}(D_{\rm Coul})\frac{\sigma_{\rm QE\ (Coul)}}{\sigma_{\rm QE}}, \tag{13}$$

where $\sigma_{\rm QE(Coul)}P_{\rm tr}(D_{\rm Coul})$ and $\sigma_{\rm QE(nuc)}P_{\rm tr}(D_{\rm nucl})$ are the individual transfer cross sections and $D_{\rm Coul}$ and $D_{\rm nucl}$ are the distances of closest approach for the Coulomb and nuclear branches, respectively. Here the transfer probability has the form given in (9) and is assumed to be constant for values of distances of closest approach smaller than D_0. Equation (13) gives us a physical picture and is valid when the contribution from one of the branches is much larger than the other and would tend to become inaccurate near the Coulomb rainbow angle. The use of the classical deflection function is restricted to angles below the rainbow angle, although larger angles can arise from the negative angle branch, but are neglected due to strong absorption in heavy-ion reactions.

As opposed to an incoherent sum as mentioned above, if a coherent addition is to be made, then a partial wave sum can be used for the transfer cross sections,

$$\frac{d\sigma_{\rm tr}}{d\Omega}=\left|\frac{i}{2k}\sum_l\ (2l+1)f_l e^{-2\beta_l^I}e^{2i\beta_l^R}P_l(\cos\theta)\right|^2, \tag{14}$$

where β_l^R, β_l^I, and f_l are the real and imaginary parts of the complex phase shift and the form factor f_l for the lth partial wave, respectively. The real parts of the phase shifts are obtained using only the real potential and the imaginary parts of the phase shifts are obtained as in Broglia and Winther [40] and using the imaginary part of the potential with $W_0=20$ MeV, $R_{0i}=8.15$ fm, and $a_0 i=0.54$ fm. The form factor f_l was assumed to be of the form $F_0 e^{-\alpha[r(l)-r_0]}$ for large distances. The results of the calculations are seen in Fig. 4 for the 110 MeV data. The curves obtained using (13) and (14) are in good agreement with the data. These calculations are similar to the quantum mechanical calculations of Wusomaa *et al.* [41] but they used Coulomb phase shifts for the real part of the phase shifts and $f_l e^{-2\beta_l^I}$ was parametrized. The calculations presented above have an uncertainty for large angles as f_l is not well known for small distances. The effect of the imaginary part of the potential on the trajectory can be large for small distances (impact parameter) and hence the calculations for small distances are not made.

To reiterate the reliability of the semiclassical calculations a comparative study of the elastic scattering obtained from semiclassical and quantum mechanical methods was made. For this purpose the relationship between the phase shifts and the deflection angle as given by

$$\theta(l)=2\,{\rm Re}\left(\frac{d\beta_l}{dl}\right) \tag{15}$$

was used. The quantal deflection function was obtained from (15). The quantum mechanical phase shifts for elastic scat-

tering were obtained from the code ECIS [42]. For the regions of interest it was seen that the quantal and semiclassical deflection functions agreed quite well [43]. The elastic scattering cross sections were also obtained using complex turning points in the WKB expression [44] for the phase shifts. The differential cross sections for elastic scattering, obtained from the above-mentioned methods, agree well with each other, except for very large angles where the perturbative method is not a good approximation [44] and is known to fail.

In the calculations of quasielastic scattering a phenomenological optical potential was employed, ignoring deformation dependence, as the purpose was to understand the transfer process in a simple way. The effect of deformation in the increase in the transfer cross section has been studied [45] and was not the subject of the present investigation. In the present analysis quasielastic scattering is treated as an incoherent sum of the various processes [15]. The value of α (the slope of the $P_{\rm tr}$ vs D graph) is related to the binding energy of the transferred particle (provided only one distance contributes at a given angle). Corrections for the Coulomb effects (for charge particle transfer) and also for the excitation in the target and projectile are required. An idea of how the excitation energy is shared between the target and projectile which is required for corrections to be made in α cannot be made from the measurement of a Q-value spectrum alone. For asymmetric systems the Coulomb correction is substantially different for the initial and final states and a simple averaging would be an oversimplification. Some of the questions raised by Liang *et al.* [37] related to the difference in neutron and proton transfer could be connected to the above.

In the present approach where the transfer probability was obtained as a sum of the contribution of the two branches, the treatment is perturbative in terms of W, the imaginary part of the optical potential. More rigorous calculations using the complex WKB method where the effect of W is treated exactly and the transfer probability can still be expressed as a coherent sum of the various contributions would give improved results. Such calculations using the saddle point integration method can be made, bringing out the contributions from the various branches in a very elegant way. Calculations using complex impact parameters as in [38] as opposed to the complex l integration [39] have been made for elastic scattering [46] and those for transfer are in progress.

After understanding the distance dependence of the measured transfer probabilities, in the next section we shall utilize it to obtain the strength of the form factors for the transfer channels required in a coupled channel calculation for fusion.

B. Fusion

The measured fusion cross section and average angular momentum are compared with the neutron flow model of Stelson [17] and the simplified coupled channel model of Dasso *et al.* [12]. The connection between these seemingly different models was pointed out by Rowley *et al.* [47] where the macroscopic description for neutron flow and neck formation was shown to be related to the microscopic coupled channel calculations for neutron transfer channels.

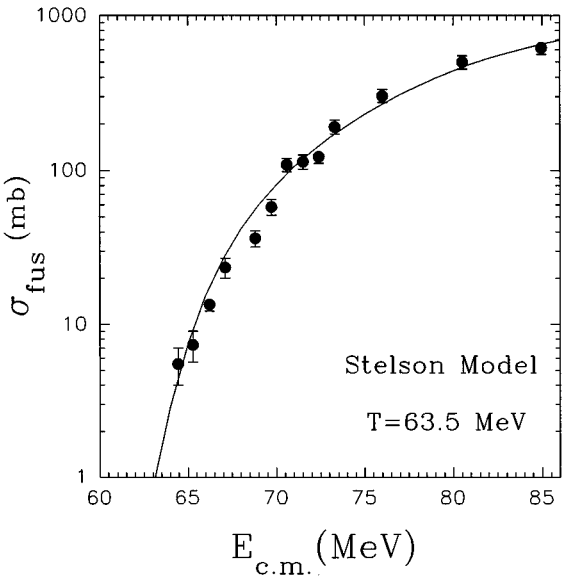

FIG. 11. The experimental fusion cross section as function of the center-of-mass energy in the ^{19}F + ^{165}Ho system. The solid line shows the calculations using the Stelson model with a threshold barrier $T = 63.5$ MeV.

1. Stelson model

The Stelson model, which is a macroscopic model, attributes the enhancement to the onset of neutron flow due to exchange of neutrons between the interacting nuclei (eventually leading to fusion) at a distance larger than the barrier radii. From an analysis of data for a large number of systems, Stelson empirically found that a flat distribution of barriers, $D(B)$, with a cutoff at a threshold barrier (T) were required to fit the data for energies below the barrier. The fusion cross section is assumed to be given by

$$\sigma_{\rm fus}(E) = \int_0^\infty \sigma_{\rm fus}(E,B) D(B) dB, \tag{16}$$

where

$$\sigma_{\rm fus}(E,B) = \pi R_b^2 \left(1 - \frac{B}{E}\right). \tag{17}$$

In our calculations we have used a quantum mechanical form for $\sigma_{\rm fus}(E,B)$ instead of the classical one. The threshold barrier T has been determined by fitting the data at near-barrier energies as suggested by Stelson. The distance at which the threshold barrier occurs in the internucleon potential is supposed to be the distance at which the least-bound neutrons may flow from one nucleus to the other. This can be calculated to be the distance where the maximum value of the merged neutron potential (obtained assuming a neutron shell-model potential centered on each of the interacting nuclei [17]) is deeper than the binding energy of the valence neutron of the two interacting nuclei. The validity of this model and the justification that transfer of one or two nucleons is the doorway to fusion have been more critically explored in a recent paper [48]. Shown in Fig. 11 is a comparison of the fusion data with the Stelson model. The barrier parameters are the same as those for the coupled channel calculations.

TABLE I. Ground state Q values in MeV of the various transfer channels. The + refers to pickup and − refers to stripping channels, respectively.

Channel	Q_{gg} (MeV)	Channel	Q_{gg} (MeV)	Channel	Q_{gg} (MeV)	Channel	Q_{gg} (MeV)
-1p	-0.68	-1n	-4.19	+1p	6.63	+1n	-1.39
-2p	-11.72	-2n	-6.054	+2p	0.46	+2n	0.04
-α	-5.22	+α	10.61	+1p1n	5.73	+1p2n	9.82

The value of T obtained was 63.5 MeV. Using the distance at which the neutron transfer was possible from the merged shell-model potentials, T was found to be 63.8 MeV.

2. Coupled channel model

It was pointed out by Dasso *et al.* [12] that the coupling of the incident channel to other channels such as inelastic and transfer modifies the barriers. By calculating the transmission through the new barriers (with their appropriate weights) the fusion cross section can be obtained. The change in height and the weights of these new barriers depend on the strength of the couplings $F_i(r)$ of the ith state to the ground state and the Q value for that state. To simplify calculations they had suggested the use of the constant coupling approximation (with improvements); that is, the r dependence of $F_i(r)$ is neglected and is replaced by its representative value $F_0 = F(R_b)$, where R_b is the barrier radius for a given system.

As seen from Fig. 8 the measured fusion cross sections are found to be enhanced as compared to a one-dimensional barrier penetration model (1D BPM) using a WKB approximation for a parabolic barrier and an incoming boundary wave condition for fusion. In this work the Woods-Saxon parametrization for the nuclear potential of Broglia and Winther [40] was modified to fit the high-energy fusion data (V_0=77.51 MeV, R_0=9.6 fm, a_0=0.66 fm). The corresponding barrier parameters are V_b = 71.4 MeV, R_b = 11.41 fm, and $\hbar\omega$= 4.35 MeV. Calculations were made using a modified version of the coupled channel code CCDEF [49,50].

These calculations, in the case of static deformation, do not take into account the finite excitation energy of the various excited levels in the rotational band. This leads to a poor approximation and results in an overprediction of the fusion cross section. This is especially true for the lighter projectile where the energy levels are quite high. Because of this reason, instead of treating ^{19}F as statically deformed, five inelastic states were coupled [51]. A deformation parameter β_2= 0.3 was used for the target [16]. The extraction of the strength of the form factors for the transfer reaction channels was done as follows: The form factor was assumed to have the form $F(r)=F_0 e^{\alpha(r-r_b)}$ for $r>R_b$, where F_0 is the value at the barrier radius. From a first-order approximation to a semiclassical coupled channel description of heavy-ion reactions [40] the transfer probability to given state β having a Q value Q_β can be related to the form factor F_β [52,53] as

$$P_{\rm tr}(D_0,Q_\beta)=\frac{\pi}{\sigma^2}|F_\beta(D_0,Q_\beta)|^2\exp\left\{-\frac{(Q_\beta-Q_{\rm opt})^2}{2\sigma^2}\right\}. \tag{18}$$

The value of $P(D_0)$ was obtained on explaining the data using (13). The effective coupling strengths F_0 were then obtained from (18). The experimentally observed values of σ, the width of the Q distribution, were used. The F_0 values thus obtained were then used in the coupled channel calculation for the fusion cross section and average angular momentum in the ^{19}F + ^{165}Ho system. Listed in Table I are the important transfer channels and their ground state Q values. Given in Table II are the values of F_0, Q, and α for the various transfer channels in the calculation. The values of α have been calculated by averaging over the initial and final channels after correcting for Coulomb effects (in the case of charged particle transfer) and for the excitation energy [53]. The pickup channels have large positive Q values. From the measured transfer probabilities at 110 MeV for the $z+1$ pickup channels, consisting of the $1p$, $1p1n$, and $1p2n$, an upper limit on the strength of the coupling was obtained and used in the coupled channel calculation. The calculation did not include coupling to the $+2n$ channel as this channel was not observed experimentally. Figure 8 shows the results of CCDEF calculations with static deformation and inelastic and transfer couplings. From Figs. 8 and 9 it can be seen that the coupled channel calculation with the inclusion of the important channels agrees well with the data.

TABLE II. Coupling strengths F_0, Q values, and values of the slope parameter α used in the coupled channel calculations.

Channel	α (fm^{-1})	Q (MeV)	F_0 (MeV)
-1p	0.73	-9.61	0.87
-2p	1.71	-19.56	0.57
-α	1.56	-19.56	1.25
+1p	0.81	1.5	1.42
+1n	0.43	-2.7	0.43
-1n	0.43	-4.5	0.76

IV. SUMMARY

A complete study of the $^{19}F + {}^{165}Ho$ system consisting of the fusion cross section, average angular momentum, and transfer probability measurements has been made at energies around the Coulomb barrier.

The average angular momentum obtained by three different methods agrees within the experimental uncertainties, establishing the validity of the assumptions involved. In the estimation of l from the fusion excitation function, using a discrete data set, it is implicitly assumed that the fusion cross section is a smooth function of energy. Measurements made at closer spaced energies would result in greater confidence in the extracted l. As l is derivable in a model-independent way from the fusion excitation function, separate measurements for l may not be required.

The fusion data could be fitted with the Stelson model and as suggested by the model, a good correlation between the threshold barrier and the distance at which the neutron flow is possible was obtained.

Coupled channel calculations were made using well-understood couplings to the inelastic channels in the projectile and static deformation for the target. The strengths of the required form factors for the transfer channel necessary in the coupled channel calculations of fusion were extracted from the measured transfer data. This was done after understanding the distance dependence of the transfer process in an improved semiclassical method considering contributions from both the Coulomb and nuclear branches of the classical deflection function. These calculations for the fusion cross-section enhancement reiterate the major role played by the static deformation of the target. The role of projectile excitations and transfer channels seems to be comparable. Both the fusion cross section and the average angular momentum are simultaneously explained within the above coupled channel calculations.

More exact coupled channel calculations may be required for the simultaneous and consistent understanding of the various processes involved. As such calculations are very difficult in a quantum mechanical approach, a semiclassical approach may be a more appropriate choice.

ACKNOWLEDGMENTS

We would like to thank C.V.K. Baba for many useful suggestions. Fruitful discussions with D.R. Chakrabarty, V.M. Datar, B.K. Nayak, and S. Suryanaryana are acknowledged. We also thank D.C. Ephraim for making the targets and the Pelletron accelerator staff for their untiring efforts in delivering the ion beams.

[1] W. Reisdorf, J. Phys. G **20**, 1297 (1994).
[2] M. Beckerman, Rep. Prog. Phys. **51**, 1047 (1988).
[3] R. Vandenbosch, Annu. Rev. Nucl. Part. Sci. **42**, 447 (1992).
[4] C.H. Dasso, H. Esbenson, and S. Landowne, Phys. Rev. Lett. **57**, 1498 (1986).
[5] A.B. Balantekin and P.E. Reimer, Phys. Rev. C **38**, 379 (1986).
[6] K.E. Rehm, Annu. Rev. Nucl. Part. Sci. **41**, 429 (1991).
[7] D.R. Napoli, A.M. Stefanini, H. Moreno Gonzalez, B. Million, G. Prete, P. Spolaore, M. Narayanaswamy, Zi Chang Li, S. Beghini, G. Montagnoli, F. Scarlassara, G.F. Segato, C. Signorini, F. Soramel, G. Pollarolo, and A. Rapisarda, Nucl. Phys. **A559**, 443 (1993).
[8] R.A. Broglia, C.H. Dasso, S. Landowne, and A. Winther, Phys. Rev. C **27**, R2433 (1983); R.A. Broglia, C.H. Dasso, S. Landowne, and G. Pollarolo, Phys. Lett. B **133**, 34 (1983).
[9] R.A. Broglia and A. Winther, Phys. Rep. C **4**, 153 (1972); R.A. Broglia, S. Landowne, R.A. Malifliet, V. Rostokin, and A. Winther, Phys. Rep. C **11**, 1 (1974).
[10] M.V. Berry and K.E. Mount, Rep. Prog. Phys. **35**, 315 (1972).
[11] G.R. Satchler, M.A. Nagrajan, J.S. Lilley, and I.J. Thompson, Ann. Phys. (N.Y.) **178**, 110 (1987).
[12] C.H. Dasso, S. Landowne, and A. Winther, Nucl. Phys. **A405**, 381 (1983); **A407**, 221 (1983).
[13] R.A. Broglia, G. Pollarolo, and A. Winther, Nucl. Phys. **A361**, 307 (1981); G. Pollarolo, R.A. Broglia, and A. Winther, *ibid.* **A406**, 369 (1983).
[14] C.H. Dasso and G. Pollarolo, Phys. Lett. B **155**, 223 (1985).
[15] C.V.K. Baba, V.M. Datar, K.E.G. Löbner, A. Navin, and F.J. Schindler, Phys. Lett. B **338**, 147 (1994).
[16] J. Christely, R.C. Johnson, and I.J. Thompson, J. Phys. G **20**, 169 (1994).
[17] P.H. Stelson, Phys. Lett. B **205**, 190 (1988).
[18] A. Chatterjee, S. Kailas, S.S. Kerakette, A. Navin, Suresh Kumar, C. Badrinathan, and A. Roy, in Proceedings of the DAE Symposium [Nucl. Phys. **32**, P-62 (1989)].
[19] R.D. Patil, A.K. Jethra, M.D. Ghodgaonkar, and A. Chatterjee, in Proceedings of the DAE Symposium [Nucl. Phys. **37**, 431 (1994)]; and (unpublished).
[20] L.C. Northcliff and R.F. Shilling, Nucl. Data Tables A **7**, 233 (1970).
[21] A. Navin, A. Chatterjee, S. Kailas, A. Shrivastava, P. Singh, and S.S. Kapoor, in Proceedings of the DAE Symposium [Nucl. Phys. **36**, 157 (1993)].
[22] R.B. Roberts, S.B. Gazes, J.E. Mason, M. Satteson, S.G. Teichmann, L.L. Lee, Jr., J.F. Liang, J.C. Mahon, and R.J. Vojtech, Phys. Rev. C **47**, R1831 (1993).
[23] *Table of Isotopes*, 7th ed., edited by C. Michael Lederer and Virginia S. Shirley (Wiley, New York, 1978); U. Reus and W. Westmeir, At. Nucl. Data Tables **29**, 1, 193 (1983).
[24] F. Pühlhofer, Nucl. Phys. **A280**, 267 (1977).
[25] B.K. Nayak, R.K. Choudhury, L.M. Pant, D.M. Nadkarni, and S.S. Kapoor, Phys. Rev. C **52**, 3081 (1995).
[26] S. Van der Werf, Nucl. Instrum. Methods **153**, 221 (1978); W.J. Ockels, Z. Phys. A **286**, 181 (1978).
[27] S. Gil, R. Vandenbosch, A. Charlop, A. Garcia, D.D. Leach, S.J. Luke, and S. Kailas, Phys. Rev. C **43**, 701 (1991).
[28] M. Dasgupta, A. Navin, Y.K. Agarwal, C.V.K. Baba, H.C. Jain, M.L. Jhingan, and A. Roy, Phys. Rev. Lett. **66**, 1414 (1991).
[29] C.V.K. Baba, in Proceedings of The International Nuclear Physics Conference, Wiesbaden, Germany, 1992 [Nucl. Phys. **A553**, 672c (1993)]; C.V.K. Baba and A. Navin, in Medium

Energy Heavy Ion Accelerator Facility (B.A.R.C - T.I.F.R) Report: July 1989–December 1992, edited by M.A. Eswaran and P.N. Tandon, 1993 (unpublished).
[30] F.G. Perey, Phys. Rev. **131**, 745 (1963).
[31] D. Wilmore and P.E. Hodgson, Nucl. Phys. **55**, 673 (1964).
[32] J.R. Huizenga and G. Igo, Nucl. Phys. **29**, 242 (961).
[33] W. Dilg, W. Schantl, H. Vonach, and M. Uhl, Nucl. Phys. **A217**, 269 (1973).
[34] A. Charlop (private communication).
[35] C.R. Morton, D.J. Hinde, J.R. Leigh, J.P. Lestone, M. Dasgupta, J.C. Mein, J.O. Newton, and H. Timmers, Phys. Rev. C **52**, 243 (1995).
[36] K.E. Rehm, B.G. Glagola, W. Kutschera, F.L.H. Wolfs, and A.H. Wuosmaa, Phys. Rev. C **47**, 2731 (1993).
[37] J.F. Liang, L.L. Lee, Jr., J.C. Mahon, and R.J. Vojtech, Phys. Rev. C **50**, 1550 (1994).
[38] J.F. Knoll and R. Schaeffer, Ann. Phys. (N.Y.) **97**, 307 (1976).
[39] E. Vigezzi and A. Winther, Ann. Phys. (N.Y.) **192**, 432 (1989).
[40] R.A. Broglia and A. Winther, *Heavy Ion Reactions* (Addison-Wesley, Redwood City, CA, 1991), Vol. 1.
[41] A.H. Wuosmaa, K.E. Rehm, B.G. Glagola, Th. Happ, W. Kutschera, and F.L.H. Wolfs, Phys. Lett. B **255**, 316 (1991).
[42] J. Raynal, Phys. Rev. C **23**, 2571 (1981).
[43] N.K. Glendenning, Rev. Mod. Phys. **47**, 659 (1975).
[44] T. Koeling and R.A. Malifliet, Phys. Rep. C **22**, 181 (1975).
[45] S. Landowne and C.H. Dasso, Phys. Lett. B **202**, 31 (1988).
[46] C.V.K. Baba and A. Navin (unpublished).
[47] N. Rowley, I.J. Thompson, and M.A. Nagarajan, Phys. Lett B **282**, 276 (1992).
[48] D. Shapira and P.H. Stelson, Phys. Rev. C **47**, 1666 (1993).
[49] J. Férnandez-Niello, C.H. Dasso, and S. Landowne, Comput. Phys. Commun. **54**, 409 (1989).
[50] M. Dasgupta, A. Navin, Y.K. Agarwal, C.V.K. Baba, H.C. Jain, M.L. Jhingan, and A. Roy, Nucl. Phys. **A539**, 351 (1992).
[51] M. Oyamada, T. Terasawa, K. Nakahara, Y. Endom, H. Saito, and E. Tanaka, Phys. Rev. C **11**, 1578 (1975).
[52] S. Saha, Y.K. Agarwal, and C.V.K. Baba, Phys. Rev. C **49**, 2578 (1994).
[53] L. Corradi, S.J. Skorka, U. Lenz, K.E.G Löbner, P.R. Pascholati, U. Quade, K. Rudolph, W. Schomburg, M. Steinmayer, H.G. Theis, G. Montagnoli, D.R. Napoli, A.M. Stefanini, A. Tivelli, S. Beghini, F. Scarlassara, C. Signorini, and F. Soramel, Z. Phys. A **334**, 55 (1990).